SECTION 3. ELECTRICAL ENGINEERING

10.46299/ISG.2022.MONO.TECH.4.3.1

3.1 Aspects related to the improvement of the technology of applying physical and mathematical models to increase the electromagnetic stability of aerospace engineering samples

The relevance of ensuring the electromagnetic stability of aerospace engineering samples is constantly growing due to the use of electronic components with a low level of resistance to powerful interference, which is due to the use of an elemental base created by nanotechnology. In addition, increasingly responsible functions (control, management, decision-making, etc.) rely on devices containing such components. On the other hand, the level of electromagnetic "pollution" of the surrounding space is steadily increasing. Moreover, to the natural sources of powerful electromagnetic disturbances, for example, caused by lightning discharges, with a certain probability, sources of artificial origin can be added, especially during military conflicts.

The level of resistance to electromagnetic interference (interference immunity level) is defined as the maximum level of a certain electromagnetic interference affecting a specific technical device, at which it (the device) retains the ability to function with the required quality. Depending on the scope of application of the device sample, the level of its interference resistance is determined. Confirmation of the specified level (certification) is carried out only experimentally according to the established methods (separate for each type of powerful disturbances).

The use of physical and mathematical modeling during design and factory testing can significantly reduce costs and time to ensure the required level of resistance of aerospace equipment to powerful electromagnetic interference. The scientific basis of improving the technology of involving physical and mathematical models to increase the electromagnetic stability of aerospace engineering samples and the methods and means of measuring the parameters of the relevant electrophysical processes are considered.

The experience of operating aerospace facilities shows that one of the most difficult tasks associated with achieving the required level of reliable and high-quality functioning is ensuring the stable operation of their electronic equipment (EE) in a complex interfering electromagnetic environment (EMO) (environments of influence various electromagnetic disturbances, especially powerful ones), which are generated by sources of natural and artificial origin. Electromagnetic interference is an unwanted physical phenomenon or the influence of electric, magnetic or electromagnetic fields, electric currents or voltage from an external source, which disrupts the normal operation of technical means, or causes deterioration of the technical characteristics and parameters of these means [209]. Power electromagnetic interference (PEMI) is interference that can lead to irreversible processes in the elemental base of EE, failures and (or) failure of this device [210]. The criteria for the operation of EE in such conditions of exposure to electromagnetic interference of any kind are defined as follows [211]:

A – normal functioning in accordance with the specification;

B – temporary deterioration of the quality of functioning, which disappears after the termination of the interference;

C – temporary deterioration of the quality of functioning, the correction of which requires operator intervention or system restart;

D – failure or irreversible deterioration of the quality of functioning of the EE, due to damage to hardware or software, or loss of data;

E - degradation that can cause fire safety problems.

In other words, the violation of the normal functioning of the EE in complex obstructive EMO has a reversible and irreversible nature. Reverse disturbances are mainly associated with the destabilizing effect of electromagnetic interference on radio and electrical equipment and the deterioration of the quality of their functioning. Irreversible violations lead to emergency situations, failures and failure of these facilities. This especially applies to the influence of unintentional and organized powerful electromagnetic interference (PEMI) of natural and artificial origin. In contrast to radio noise, the influence of PEMI on EE is highly likely to be associated with impairment of the performance of these means up to the occurrence of irreversible processes in their elemental base, and as a result - partial failures or complete failure of radio and electrical equipment. Such situations are the result of either the direct impact of current and voltage of electromagnetic interference in the external and internal elements of structures, circuits and circuits of radio and electrical equipment, or the occurrence of voltage and current induced by electromagnetic fields in them. These voltages and currents often exceed the maximum permissible levels stipulated by the operating conditions of the EE, which can lead to the local release of a significant amount of heat on the elements, which ultimately causes their melting and burning, or electrical failure of the EE elements. According to the form of interference, they are divided into impulse and regular [210]. Impulse disturbances are single pulses (signals concentrated in time) or their sequence, arbitrary in shape and different in amplitude, which appear at random moments of time, and, for a sequence of pulses, the intervals between them are, as a rule, longer than the duration of the pulses themselves. Regular disturbances are defined as harmonic and oscillatory.

It is difficult to determine the exact quantitative limit between radio interference and powerful electromagnetic interference. Thus, in [212] it is noted that the degree of influence on crystal mixers and detectors of radar receivers depends on the total energy of interference pulses with a duration of less than 10 ns. Interference energy in the range of (0.1 - 1.0) μJ causes burnout of semiconductor devices used in the frequency range from 1 to 10 GHz. For semiconductor devices used at higher frequencies, burnout levels vary between (0.01 - 0.1) μJ. The effect of single pulses longer than 10 ns depends on their power. Failure of devices used at frequencies below 10 GHz usually occurs at maximum (pulse) power levels above 5 W. Equipment designed to operate at higher frequencies fails at pulse power levels above 0.5 W. Deterioration of quality, which occurs under the action of a sequence of pulses, occurs at significantly lower power levels than in the case of a single pulse. A typical level of such power for a sequence of pulses is 1% of the power of a single pulse [212, 213]. Depending on the type and nature of the radiation sources, PEMZ sources are divided into two classes: interference of natural and artificial origin. Disturbances of natural origin are not related to human life processes and occur independently of them. Disturbances of artificial origin, created artificially with the help of purposeful human activity, belong to the class of organized and are created to impair the quality of functioning or disable the EE.

The most common sources of PEMI of natural origin, which are subject to mandatory regulation, include various manifestations of the influence of lightning discharges. Among the sources of organized PEMI of artificial origin, the striking effect of which causes a violation of the quality or failure of EE, and the parameters of which must also be regulated, include nuclear explosions (HEMP). According to the classification given in the International Standard IEC 61000-2-5 [214], a disruptive electromagnetic environment that has a striking and destabilizing effect on technical means of civilian use is characterized by a power flow density of not less than 26.5 W/m2 in free space (100 V/m or 0.27 A/m).

It should be pointed out that the parameters of PEMI depend on a number of circumstances, so they are not deterministic. However, for the purpose of reproducibility of test results, specific values are determined taking into account the probability of their occurrence.

Consider the parameters of electromagnetic effects accompanying indirect lightning strikes. There are two types of electromagnetic influence on a technical device: the near and far zone of field formation. The near zone is determined by the distance from 10 m to 100 m from the discharge channel, the far zone is more than 100 m. The maximum, from the point of view of destabilizing action, time parameters of the electromagnetic field that occurs as a result of a lightning strike in the near zone at a distance from the object 10 m, shown in Table 1. It is noted that the minimum distance between the object and the lightning channel is 10 m. Distances less than 10 m are considered as a direct strike event.

Table 1.

Growth rate parameters [215]

Field type	Front growth rate
Magnetic field	$2.2 \cdot 10^{9}$ $A \cdot m^{-1} \cdot s^{-1}$
The electric field	$6,8 \cdot 10^{11}$ $V \cdot m^{-1} \cdot s^{-1}$

Standard [7, tab. 8] establishes that the rate of increase of the magnetic field strength when simulating a "cloud-ground" lightning discharge should be $2.2 \cdot 10^9$ $A \cdot m^{-1} \cdot s^{-1}$. This value is determined by assuming that the lightning channel is vertical relative to the ground surface, the lightning current 200 kA, the dependence of the current on time corresponds to component A, and the distance to the lightning channel is 10 m. The magnetic field is calculated based on Ampere's law.

$$\dot{H}(t) = \dot{I}(t) / 2\pi r$$

where r is the distance from the lightning channel to the observation point located on the Earth's surface, the dots above the letter designations of physical quantities (magnetic field strength and current) denote the time derivative.

The amplitude-time parameters of component A of the lightning current, given in Table 2, are determined for the pulse form, in the form of a unipolar pulse (Fig. 1), which allows you to control the correctness of the calculations of the time derivative (crossing through zero at the maximum current).

Table 2.

Characteristics of forms of indirect effects of lightning [215]

Current compo-nent	Peak current (kA)	Action Integral (A^2s)	Decay to 50% (μs)	Time to 10% (μs)	Time to 90% (μs)	Time to Peak (μs)	Rate of rise (A/s)	Peak rate of rise t = 0+ (A/s)
A	200	$2.0x10^6$	69	0.15	3.0	6.4	$1.0x10^{11}$ @ 0.5 μs	$1.4x10^{11}$
B	Produces average current of 2 kA over a 5 millisecond period							
C	Defined as rectangular waveform for analysis purposes of 400 A for 500 milliseconds							
D	100	$0.25x10^6$	34.5	0.08	1.5	3.18	$1.0x10^{11}$ @ 0.25μs	$1.4x10^{11}$
D/2	50	$6.25x10^4$	34.5	0.08	1.5	3.18	$0.5x10^{11}$ @ 0.25μs	$0.7x10^{11}$
H	10	N/A	4.0	0.0053	0.11	0.24	N/A	$2.0x10^{11}$

Table 2 shows the other components of the lightning current, which correspond to various options for the interaction of lightning with the aircraft. These features should be taken into account during the general assessment of the level of EE immunity. Component A is the most powerful, so only it is considered further.

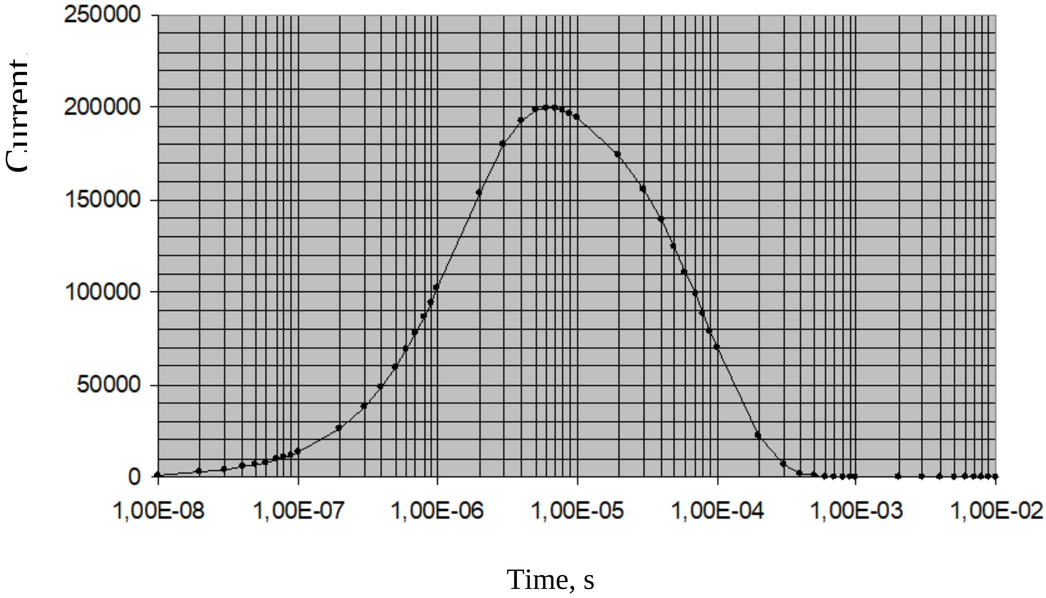

Figure 1. The shape of the time dependence of the A component of the lightning current

To find the maximum value of the increasing speed of the magnetic field intensity, the time derivative of the lightning current was calculated. The result of the calculation is presented in Figure 2.

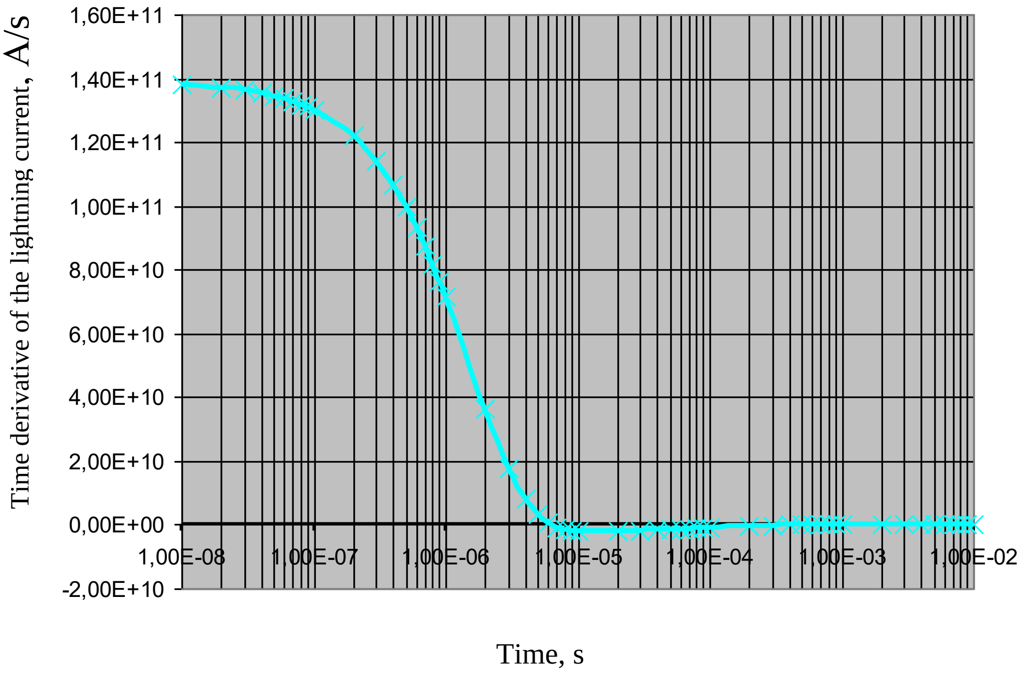

Figure 2. Derivative component A of the lightning current

Figure 1.2 shows that the current pulse has a maximum growth rate of $1.4 \cdot 10^{11}$ A/s (at a current of $2 \cdot 10^5$ A), which corresponds to the data recorded in Table 2 for component A.

Dividing the value of the maximum rate of increase of the current strength by 62.8 (2πR, R = 10 m), we get $2.23 \cdot 10^9$ $A \cdot m^{-1}s^{-1}$, the value specified in Table 1 for the magnetic field strength. The algorithm for calculating the magnetic field intensity level is important because it allows you to determine the limit parameters for the EO sample, taking into account its technical features (overall dimensions, surrounding objects, lightning protection systems). It should be noted that the above-mentioned value of the rate of increase of the magnetic field intensity is the maximum possible, based on the formulas given in the standard, which describe the time dependence of the current strength in the lightning channel. This value is reached at time t = 0 +. In reality, the current does not increase at the moment of "turning on" by a jump, and always has a section of smooth increase. Therefore, when determining the parameters of the magnetic field strength, which must be implemented for the purposes of testing, it is advisable to proceed from the value of the average growth rate, which is obtained as a result of dividing the difference in the strength values at the levels 0.1-0.9 by the maximum value $\Delta I_{0.1\text{-}0.9}$ for the time interval between the moments of reaching these values $\Delta t_{0.1\text{-}0.9}$. In this case, the value of the rate of increase of the magnetic field strength at a distance of 10 m will be equal to $8.9 \cdot 10^8$ $A \cdot m^{-1}s^{-1}$, which is 2.5 times less than indicated in Table 1. In addition, it is possible to choose the value of the speed the increase of the magnetic field based on the value of the rate of increase of the current strength of $1.0 \cdot 10^{11}$ $A \cdot s^{-1}$, which is reached at a time of 0.5 μs, as can be seen from Figure 1.2 and the data in Table 2. Based on the maximum requirements of the standard [215], when testing the sample, the goal of achieving the value of the rate of increase of the magnetic field intensity is $2.23 \cdot 10^9$ $A \cdot m^{-1}s^{-1}$. Taking into account the above, it is enough to set the pulse of the magnetic field intensity in a time form that is similar to the form of the A component of the lightning current.

It should be noted that there is a contradiction between the two basic standards [215] and [216] regarding the parameters of the electric field. Section 254.4 of the

AESTR-250 standard [216] is devoted to consideration of the form of amplitude-time parameters and the effects of direct and indirect lightning strikes, which are used in lightning resistance tests. Indirect lightning strikes are lightning discharges at a distance of at least 10 m from the object and are characterized by electric and magnetic fields. The strengths of these fields are given in the AESTR-250 standard [216]. We compare the requirements for the electrical component.

The technical requirements for test electric fields given [216] are characterized by the intensity E according to formula (1) and the rate of increase of the electric field according to formula (2):

$$E = 3 \times 10^6 / \left(1 + R^2 / 50^2\right)^{1/2}, \tag{1}$$

where: E is the amplitude of the vertical component of the electric field, V/m;

R is the distance from the lightning discharge channel, m.

$$dE / dt = 6 \times 10^{12} / \left(1 + R^2 / 50^2\right)^{1/2}. \tag{2}$$

The distance R during tests must be at least 10 m from the lightning discharge channel. Thus, the maximum value of the electric field growth rate at R = 10 m is $5.88 \cdot 10^{12}$ $V \cdot m^{-1} \cdot s^{-1}$, and at a distance of 50 m it is $4.28\ 10^{12}$ $V \cdot m^{-1} \cdot s^{-1}$. It should be noted that in table 8 of the US military standard MIL-STD-464C:2010 [215], another value of the electric field growth rate is given: $E = 6.8 \cdot 10^{11}$ $V \cdot m^{-1} \cdot s^{-1}$, that is, almost an order of magnitude less. In the standard DSTU 3681-98 [217], the following characteristics of the intensity of the pulsed electric field are specified for tests:

- voltage up to 300 kV/m;
- pulse front duration – 100 μs.

The average value of the growth rate of such a pulse is $3 \cdot 10^9$ $V \cdot m^{-1} \cdot s^{-1}$. Unfortunately, the basic standard IES 62305:2010 [218] does not contain the necessary information about the electric field. We believe that the standard [216] contains erroneous requirements for electric field parameters. This conclusion is based on this assessment. The maximum value of $5.88 \cdot 10^{12}$ $V \cdot m^{-1} \cdot s^{-1}$ regulated by the standard [216] means that in 1 μs the electric field strength should increase to the value of $5.88 \cdot 10^{6}$

$V \cdot m^{-1}$. At this voltage, the breakdown of the air gap is guaranteed, because the electrical resistivity of air in a uniform electric field does not exceed $3.0 \cdot 10^{6}$ $V \cdot m^{-1}$, and in a non-uniform one - $0.5\ 10^{6}$ $V \cdot m^{-1}$. In the presence of a test sample, the electric field will be sharply inhomogeneous. In this variant, the breakdown will occur at an electric field strength of $5.0 \cdot 10^{5}$ $V \cdot m^{-1}$, which is consistent with the requirements of the standard [215]. It is obvious that the practical implementation of the requirements of the standard [216] during sample testing is not possible.

Based on the comparison of the above data from various normative documents, a conclusion was made about the inadequacy of the requirements of the standard [216]. Therefore, it was decided to accept the requirements of the standard [215] as technical parameters for the pulsed electric field. It is important that both standards [215, 216] do not regulate the test implementation procedure, but indicate the need to do it at the national level. The testing methodology in Ukraine according to the standards under consideration, developed at KhPI National Technical University, is described in [219].

For the physical and mathematical modeling of the processes of action of powerful electromagnetic influences on EE in order to increase the stability of aviation and space technology, it is necessary to determine the parameters of possible influences. In addition to the lightning discharges discussed above, the standards regulate a number of other phenomena. According to the mechanism of influence, the phenomenon is divided into the following:

- conductive, which are distributed along galvanic lines, including electric power, communication, control cables, etc.;
- field electromagnetics that act on the entire system as a whole, including directly on the electronic circuits placed in the product body.

The sources of conductive disturbances are usually processes associated with the switching of powerful equipment, for example, the start of aircraft engines, or secondary manifestations associated, for example, with the spread of lightning current on the ground, voltages and currents arising in long lines during action electromagnetic pulse of a nuclear explosion. It is clear that an adequate test is impossible in this case. Therefore, without mathematical modeling of such processes, it is impossible to obtain an objective assessment of the level of stability of on-board aircraft equipment or equipment of strategic objects. Mathematical modeling must undergo experimental testing on cables under conditions that can be implemented experimentally.

All the variety of electromagnetic phenomena described in the standards should be summarized as follows:

- single pulses;
- bundles of pulses;
- harmonic unmodulated;
- harmonic with modulation.

Each of these types has peculiarities from the point of view of the adequacy of their mathematical modeling. It is clear that modeling the effect of bursts of pulses and modulated signals is more difficult than others. Therefore, as a first step, the mathematical modulation of the influence of single pulses and unmodulated harmonic voltages is further considered. It should be noted that pulses have different time ranges: nano, micro and milliseconds.

Let's consider the parameters of the most dangerous types of electromagnetic disturbances regulated by standards. The results of a comparative analysis of the requirements of the current NATO standards [216, 220] with the requirements of the civil standard [221], which determine the levels of resistance of the on-board equipment of aircraft to the action of powerful electromagnetic interference, are shown in Table 3.

Table 3.

The strictest requirements for the level of stability of galvanic ports

Standard / part	Disturbance type	Level test signal	Form of test signal	Time or frequency parameter	Additional information*
EUROCAE ED-14G / part 20 cat. Y	Cable injection of current	to 300 мA	Modulate harmonic	from 10 kHz to 400 MHz	Table 20-2
AECTP-500:2016 / NCS08	Cable injection of pulse current	to 5A	Unipolar pulse trapezium form 2/30/2 ns	width 30 ns, tracking frequency 30 Hz	

Continuation of table 3

AECTP-500:2016 / NCS09	Cable injection of damped oscillating current	from 0,1A to 10 A	decaying sine wave	from 10 kHz to 100 MHz	
EUROCAE ED-14G / part. 22	Transient processes caused by lightning	voltage to 3200 V,	single multiple hits and flashes	according to the shape of the pulses	Table 22-2 – 22.2-4

Note: The tables indicated in the last column are contained in the standard

It should be noted that the introduction of interference directly into the galvanic port is a rather critical type of test, which is carried out in accordance with the methodology of the standard and does not require additional mathematical modeling.

Another situation arises when testing the stability of objects with significant overall dimensions to the influence of electromagnetic fields. Options regulated by standards are presented in Table 4.

Table 4.

Parameters of electromagnetic fields

Standard / part	Disturbance type	Level test signal	Form of test signal	Time or frequency parameter	Additional information*
EUROCAE ED-14G / part 20 Cat. L	Electromagnetic wave	7200 V/m	Pulse modulation	from 100 MHz to 18 GHz	Table 20-3
AECTP-500:2016 / NRS02, (aircraft)	High intensity radio frequency field (HIRF)	200 V/m	electromagnetic field, modulated sinusoid	from 2 MHz to 40 GHz	Table NRS-02-1
AECTP 250:2014 / part 258	Radio frequency electromagnetic field	Peak level to 7200 V/m	continuous or pulse modulated sine wave	from 0,01 MHz to 40 GHz	Table 258-3B
AECTP-500:2016 / NRS03	The electromagnetic pulse of a nuclear explosion (HEMP)	50 kV/m	unipolar impulse	front 2 ns, width 23 ns	

Note: The tables indicated in the last column are contained in the standard

The data shown in Table 4 give grounds for the following conclusions:

1. The formation of radio frequency fields with the specified levels of electric field strength during pulse modulation is a complex technical task, especially under the conditions of significant dimensions of the working volume. The solution costs millions of US dollars apparently for a volume of 8 m^2. The high cost is associated with the need to use a line of broadband generators, amplifiers and appropriate metrological support.

2. For large objects, such as an airplane, meeting the requirements of the standards is not possible without the use of mathematical modeling methods. In Ukraine, systematic studies in this direction have not been conducted so far.

3. It is known that cable lines are the most effective receiver of electromagnetic field energy. Therefore, one of the main aspects is the modeling of the process of EMF interaction with cables.

The on-board circuits of the aircraft are most affected by lightning currents, since their operation most often occurs in conditions of active thunderstorm activity, as a result of which these devices become the object of direct damage by lightning [222]. The direct effect of lightning currents on the aircraft is accompanied by the flow of large currents along the aircraft body and their interaction with the circuits of radio and electrical equipment located inside the aircraft. Under this electromagnetic influence of lightning currents, internal asymmetric circuits of automated control and power supply systems are most susceptible, in which the aircraft body directly acts as the return path of the current (Fig. 3). In the general case, when a lightning current $I_m(t)$ flows through it, an induced voltage consisting of resistive, inductive and aperture components (3) occur at the open ends of the asymmetric internal on-board circuit located in the fuselage (screen housing) [222].

$$U_{л}(t) = R_e l_l i_M(t) + M_{e-l} l_l \frac{di_M^*(t)}{dt} + M_B \frac{di_M^*(t)}{dt}. \quad (3)$$

where: $R_e = R_0\{1 + 2[\sum_{n=1}^{\infty}(-1)^n \, exp(-\pi^2 n^2 t/\tau_{диф})]\}$;

$i_M^*(t) = i_M(t)[1 - \exp(-t/\tau_{диф})]$, where: R_o. - resistance of a unit length of the body-screen to direct current;

$\tau_{\partial u\phi} = \mu\sigma_M d_s^2$ - time constant of lightning current diffusion into the case-screen;

$i_M^*(t)$ - lightning current flowing along the inner wall of the screen housing, taking into account the surface effect;

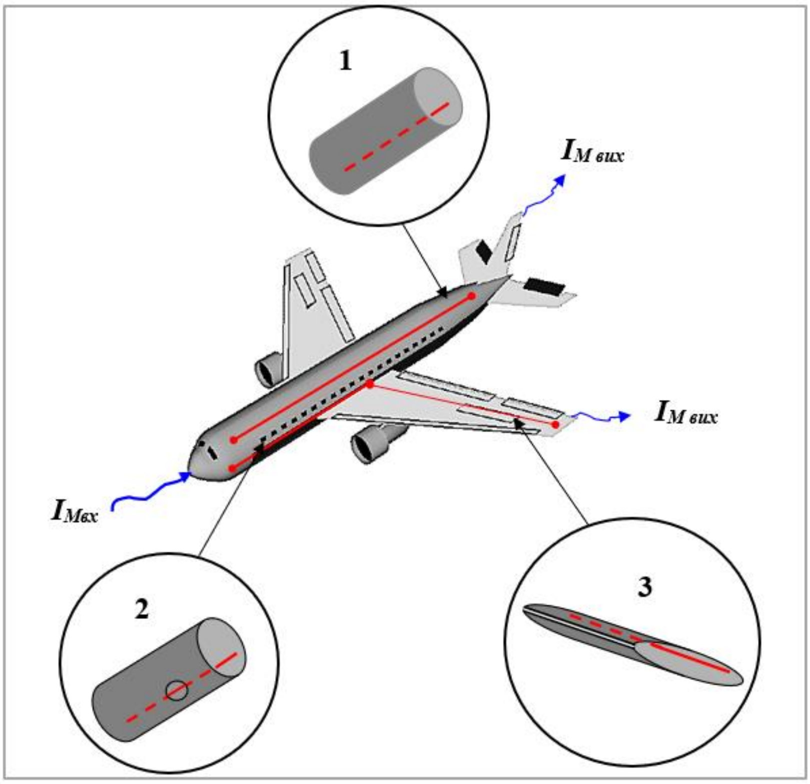

1 – homogeneous part of the cylindrical fuselage;
2 – part of the cylindrical fuselage with portholes;
3 – a wing element with a longitudinal gap formed open flaps.

Figure 3. To determine the electromagnetic influence of lightning currents flowing along the fuselage of the aircraft on its on-board circuits located in typical components of the aircraft [222]

$M_{e\text{-}l}$ is the coefficient of mutual inductance of the electrically homogeneous screen housing and the conductor of the internal circuit;

l_l – chain length;

M_B is the coefficient of mutual inductance, which is determined by the coupling flux between the conductor of the internal circuit and the external magnetic flux associated with the lightning current, which penetrates into the case-screen through electrical inhomogeneities (holes, gaps, etc.).

As practical experience shows, the most significant and difficult in calculating the voltage induced in the on-board circuits of aircraft when they are directly struck by lightning are:

- determination of the ohmic resistances of the component parts of the aircraft body (fuselage and wing) taking into account their configuration and actually existing electrical inhomogeneities in the form of gaps in the wings from shields, flaps, ailerons and holes in the fuselage from portholes and hatches;

- coefficients of mutual inductance of the aircraft body with on-board circuits laid in it and coefficients determining the effect of electrical inhomogeneities on these circuits. The dependence of the coefficient of mutual inductance between the aircraft body and the conductors of the on-board circuits on the geometric parameters is presented in Figure 4. Table 5 shows the analytical expressions obtained in [223] for determining these parameters.

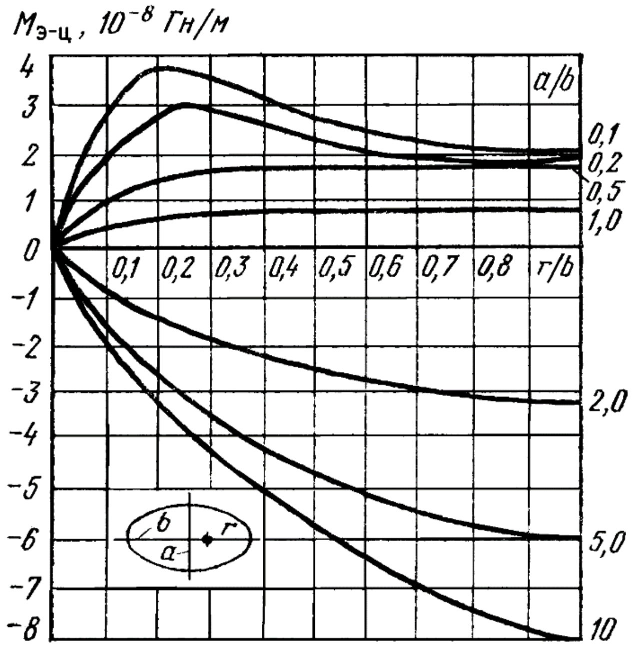

Figure 4. Dependence of the mutual inductance coefficient between the aircraft body and the conductors of the on-board circuits from the geometric parameters [223].

Table 5.

Parameters of interaction of lightning currents with on-board circuits of aircraft [223]

Aircraft component	Formulas for determining parameters	
	Direct current resistance, Ohm/m	Coefficient of mutual inductance
Homogeneous Part of the fuselage without holes (a=b), wing without open flaps (b>a)) 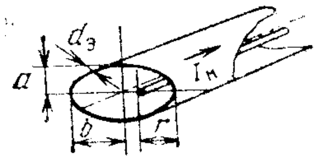	$R_{Э0} = \frac{1}{p\sigma_м d_Э}$	Look to fig. 4 for $l_e >> b$
Wing with open flaps 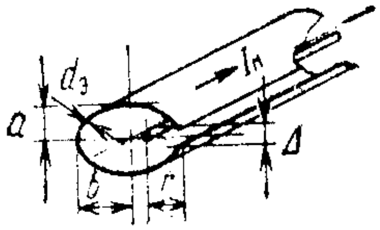	$R_{Э0} = \frac{1}{(p-\Delta)\sigma_м d_Э}$	$M_щ = \mu_0 \frac{4\Delta^2 l}{\pi}\left(\frac{2b-r}{2brp}\right)\times$ $\times\exp\left[-\left(\frac{\pi d_э}{\Delta}-2\right)\right]$, where $l = l_Ц$ if $l_Ш > l_Ц$ $l \neq l_Ц$ for $l_Ц > l_Ш$ For $r \geq \Delta$
Fuselage with portholes 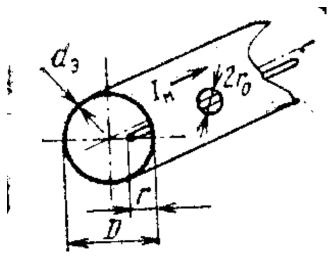	$R_{Э0} = \frac{1}{\sigma_м d_Э}\left[\frac{1}{\pi D - 2r_0}\right]$	$M_{отв} = \frac{4\mu_0 r_0^3 (D-r)}{3\pi^2 r D^2}\times$ $\times\exp\left(\frac{1,8 d_Э}{r_0}\right)$, if $r_o/r \leq 0.5\ldots0.6$ $r \leq D/2$
Note: The following designations are used in the table: $\sigma_м$ - - specific conductivity of the fuselage material, S/m; ; $p = \pi[1,5(a+b) - \sqrt{ab}]$; $l_Ц$- length of on-board chain, m; $l_Ш$- slot length, m; $l_Э$- body length, m.		

The given formulas are obtained for fairly simple options, which do not occur in practice, because the cable lines are laid in bundles and boxes. Cable laying has a complex spatial nature, usually three-dimensional. It is clear that taking into account the real parameters of the aircraft and various chains is possible only with the use of computer simulation. This process is very difficult, but necessary. Analytical dependencies can be used to check the adequacy of mathematical models by comparing the results. Developed and tested mathematical models have significant advantages because they can be applied to any object.

Let's consider the features of the impact of an electromagnetic wave propagating in free air on cable lines. Mathematical models differ depending on the ratio of the length of the cable line (CL) and the wavelength.

The mathematical description of the problem in the quasi-stationary approximation is given by the system of Maxwell's equations:

$$\begin{aligned} & rot\vec{H} = \vec{J} \\ & rot\vec{E} = -\frac{\partial \vec{B}}{\partial t} \\ & div\vec{D} = \rho \\ & div\vec{B} = 0 \end{aligned} \tag{4}$$

where $\vec{H}$ - the magnetic field intensity vector, A/m; $\vec{E}$ - electric field intensity vector, V/m; $\vec{J}$ - conduction current density vector, A/m^2; $\vec{B}$ - magnetic induction vector, T; $\vec{D}$ - electric induction vector, C/m^2; ρ - volume density of electric charge, C/m^3.

The fundamental equations are Ohm's law, the continuity equation, and Gauss's law:

$$\begin{aligned} & J = \sigma E \\ & div\vec{J} + \frac{\partial \rho}{\partial t} = 0 \\ & \nabla(\varepsilon E) = \rho \end{aligned} \tag{5}$$

Material equations are presented in the form:

$$\vec{D} = \varepsilon_0 \vec{E},$$
$$\vec{B} = \mu_0 \vec{H},$$
$$\vec{J} = \sigma \vec{E},$$

where ε_0 - the dielectric constant of vacuum, F/m; μ_0 - magnetic permeability of vacuum, H/m; σ - specific electrical conductivity, S/m.

Boundary conditions during the transition from one environment to another (dielectric - conductor) in the variant under consideration are as follows:

$$\begin{aligned} &\vec{E}_{1\tau} - \vec{E}_{2\tau} = 0 \\ &\vec{D}_{1n} - \vec{D}_{2n} = \rho_s \\ &\vec{H}_{1\tau} - \vec{H}_{2\tau} = \vec{J}_s \\ &\vec{B}_{1n} - \vec{B}_{2n} = 0 \end{aligned} \quad (6)$$

where ρ_s - surface charge density, C/m^2; $\vec{J}_s$ - surface current density vector, A/m^2.

We set the initial conditions to zero.

This formulation of the electric field distribution problem is implemented using the finite element method using, for example, the COMSOL Multiphysics AC/DC – Electrostatic module.

The mathematical description of the problem for the wave version uses a differential equation that describes the distribution of the magnetic field taking into account the displacement currents:

$$\text{rot}\, \vec{H} = \vec{J} + \frac{\partial \vec{D}}{\partial t} = \sigma \vec{E} + \vec{J}^e + \frac{\partial \vec{D}}{\partial t}, \quad (7)$$

where: J^e - external current density vector, A/m^2.

For harmonic electromagnetic fields, it is advisable to make substitutions (8), which transform the system of equations into equation (9):

$$\begin{aligned} &\vec{B} = rot\vec{A} \\ &\vec{E} = -j\omega\vec{A} \end{aligned} \quad (8)$$

$$\left(j\omega\sigma - \omega^2\varepsilon_0\right)\vec{A} + rot\left(\frac{1}{\mu_0} rot\vec{A} + \vec{M}\right) = \vec{J}^e \qquad (9)$$

where: $\vec{M}$ - magnetization vector of the material, A/m.

The differential equation (9) is the basis of the finite element calculation of the COMSOL Multiphysics AC/DC – Magnetic Fields – Frequency Domain module.

The results of the application of COMSOL Multiphysics AC/DC to determine the probability of lightning striking elements of the launcher of the Kourou Cosmodrome with the installed ARIANE 5 rocket are given in [224]. Among the results of the calculation, the magnetic field near the launch vehicle and in the areas where the equipment is located, the current on structural elements and cable lines are of interest.

When solving the problems of electric current distribution on the real body of the object and finding the electromagnetic field created by this current, it is necessary to carry out a number of stages. First, models of real objects usually created in CAD programs are characterized by high detail of all structural elements. All grooves, technological holes, surface irregularities, bolted connections and elements of the body or equipment are present in the model. It is necessary to simplify the geometry of the object in such a way as to exclude all elements that do not affect the current distribution. In most cases, this step is still not enough and a number of assumptions and approximations must be made. For example, hardware elements such as layer connections, motor design elements, etc. can be replaced by equivalent simplified designs with appropriate ohmic resistance. It is necessary to replace the real parts of the object with models while preserving the quality and detail of the model. If the geometry of the calculated model of the object will be significantly different from the original one, this may cause discrepancies with the test results. At the second stage, the simplified model is converted into the selected COMSOL Multiphysics module. At the third stage, the electrical parameters of the model elements, the operating wave parameters, and the initial conditions are set. Calculation is in progress.

The purpose of the calculation is to find the current and induced voltages on the communication cable lines. Real cables can be twisted pair, bus bars, or coaxial cable. The key role in the nature of induced voltages is played by the inhomogeneities of the object's housing, the ways of laying cable lines in the housing, and the type of cable line.

For metrological support of research and tests related to the action of powerful electromagnetic disturbances, at least the required set of measuring equipment includes the following:

- magnetic field intensity meter;
- electric field intensity meter;
- electric shunt;
- voltage divider;
- recording equipment (oscilloscope).

The conversion factors and the frequency band must correspond to the parameters of the interference under investigation. The following are the special requirements for measuring equipments.

A magnetic field strength meter is used to measure the magnetic field. Given the possible high levels of tension, the use of ferromagnetic materials should be limited.

Electric field strength meters should be a set for the entire investigated frequency range. Usually, measuring antennas (dipole, logperiodic, etc.) are used for frequencies above 1 GHz.

An electric shunt is used to measure the current in the discharge circuit of the impulse current generator. The most powerful current pulses are associated with lightning discharges, reaching 200 kA. The front of the current pulse is a unit of microseconds, so the shunt design must provide a minimum inductance (for example, a bifilar).

The voltage divider must combine a high division ratio with a high rate of rise of the transient characteristic. Usually, such dividers are made according to a mixed resistive-capacitive scheme.

For the physical modeling of the current spreading processes along the body of the object, it is advisable to have a current spreading meter to determine the magnitude of the current on the structural elements when the current is directly injected into the body of the object.

Let's consider the main regularities in the design of the magnetic field intensity meter. The electromagnetic induction method has gained widespread use due to its simplicity and reliability. Sensors based on the effect of electromagnetic induction are frame antennas in which electromotive force (EMF) is induced, according to the law of electromagnetic induction:

$$e_n = -\mu_o \mu_r S w \frac{dH_o}{dt} \cos\varphi \tag{10}$$

where: $\mu_o = 4\pi \cdot 10^{-7}$ H/m; μ_r – relative magnetic permeability; S – area of the frame, m^2; w – the number of turns; φ – the angle between the direction of the vector $\vec{H}_o$ and the normal to the frame.

Figure 5 shows the converter substitution scheme (IC), where L_d is the inductance of the converter; C_d - capacity of the converter; R_d - resistance of the converter; R_u is the resistance of the integrator, C_u is the capacity of the integrator.

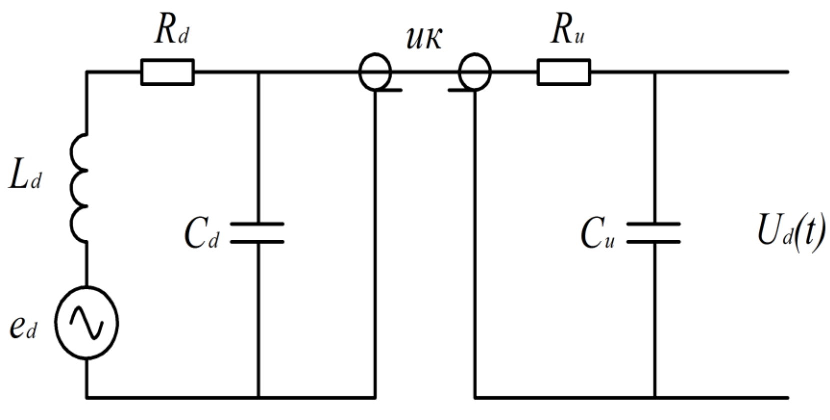

Figure 5. The scheme of replacing the induction converter

The relationship between EMF. and the voltage at the frame output U_d is described by the equation (11):

$$e_d = L_d C_d \frac{d^2 U_d}{dt^2} + \left(\frac{L_d}{R_d} + R_d C_d\right) \frac{dU_d}{dt} + \left(1 + \frac{R_d}{R_o}\right) U_d \tag{11}$$

Where: U_d – voltage at the output of the converter, which is applied to the input of the measuring cable (MC); R_0 is the MC input resistance (usually 50 ohms).

It can be seen from equation (11) that the induction-type IC is a second-order measuring transducer. As a result, the voltage at its output contains oscillating or aperiodic components superimposed on the main pulse, the amplitude and shape of which are determined by the dynamic properties of the IC. The dynamic properties of IC, intended for measuring impulse processes, are fully described by the transient characteristic.

The transient characteristic is the voltage at the output of the IC when a unit jump of the magnetic field pulse is applied to its input. For the IC, the substitution scheme of which is shown in Figure 5, the formula looks like this:

$$U_0^{TR} = \frac{R_0}{R_0 + R_d}\left[1 + \frac{1}{P_1 - P_2}(P_2 \exp(-P_1 t) - P_1 \exp(-P_2 t))\right],$$
$$P_{1,2} = -\frac{a}{2} \pm \sqrt{\frac{a^2}{4} - c},\ a = \frac{L_d + R_d R_0 C_d}{R_0 L_d C_d},\ c = \frac{R_0 + R_d}{R_0 L_d C_d}. \quad (12)$$

From equation (12) it turns out that if $a^2 < 4c$ the transient characteristic of the IC has an oscillatory character. Such IC is called uncoordinated. When $a^2 > 4c$ the transient characteristic is an aperiodic damping. In this case, it is called renegotiated. When $a^2 = 4c$ the transient characteristic will be critically coordinated, which will ensure the minimal deformation of the pulse measurement.

The rise time of the transient characteristic is estimated by formula (13)

$$T_н^{ПХ} = 3{,}35\sqrt{L_d C_d} \quad (13)$$

To obtain a signal proportional to the magnetic field, it is necessary to integrate the signal using RL - integration or RC - integration. Figure 5 shows the scheme of the IC with an RC integrator.

A TEM horn measuring transducer is used to measure short-front (sub-nanosecond) EMI parameters [225]. The design of the TEM horn measuring transducer is shown in Figure 6. The angle at the top of the triangular electrode is α , the plane of the triangular electrode forms an angle β with the horizontal plane. In some cases, a resistive coating is applied to the electrodes of the TEM horn for better matching and reducing the value of the reflection coefficient of the horn in a wide frequency band [225]. To increase the duration of the transient characteristic, the electrodes of the TEM horn are also lengthened in the form of flat parallel plates. A photograph of a TEM horn with resistive sputtering and an increased duration of the transient characteristic is shown in Figure 6.

The rise time of the transient characteristic and its duration t_x (at the zero level) can be found from formulas (14) [225]:

$$T_I^{TR} = \frac{L(1-\cos(\beta/2))\sqrt{\varepsilon}}{c},\ T_0^{TR} = \frac{2L\sqrt{\varepsilon}}{c}. \quad (14)$$

where: L – horn length (see Figure 6);

ε – relative dielectric constant of the medium inside the horn;

$c = 3 \cdot 10^8$ м / с - speed of light in vacuum.

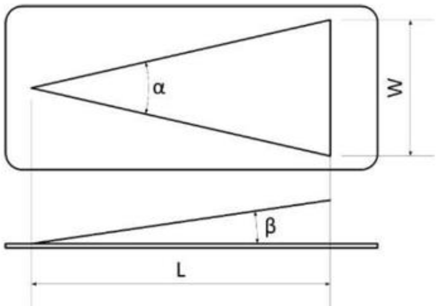

a)

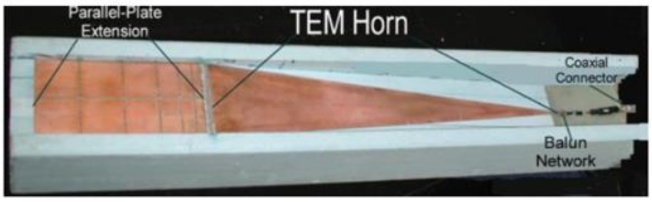

b)

(a) drawing of a TEM horn with an elongated plane-parallel part and resistive sputtering; (b) photograph of the sample [225]

Figure 6. Design of the TEM horn measuring device converter

The transient characteristic of the TEM-horn VP has the shape of a triangle with a steep front and a gentle decline [225] (Figure 7).

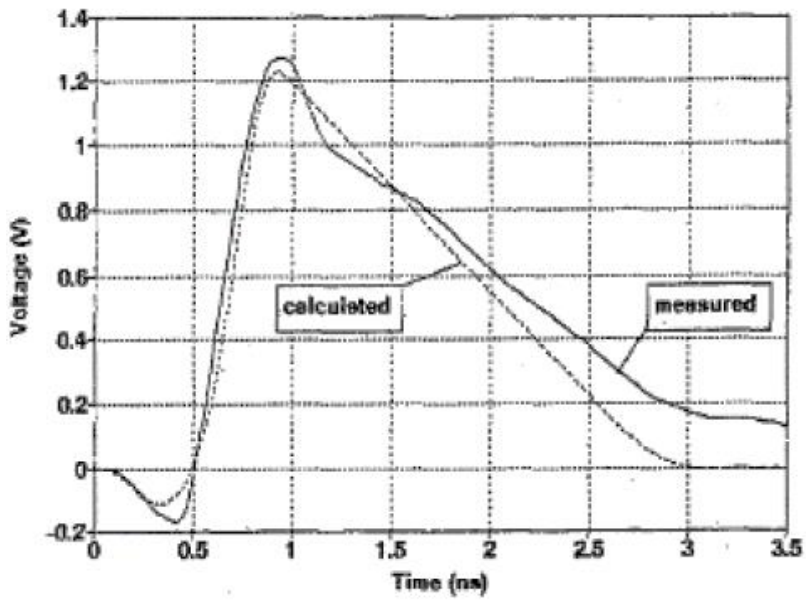

Figure 7 Transient characteristic of TEM-horn VPs [225]

In practice, the transient characteristic of the TEM-horn VP is determined during its calibration in field-forming systems that reproduce step pulses. It is possible to carry out calibration using two TEM samples [226]. Two identical loudspeakers are placed on the axis opposite each other at a distance r between the apertures (in the far radiation zone). One TEM horn is excited by a stepped signal. The electric field strength at a distance r can be found by formula (15):

$$E_0(t)=\frac{F(t)}{r}U_{in}(t), \qquad U_{in}(t)=\begin{cases}0 & t\le 0\\ 1 & t>0\end{cases}, \tag{15}$$

where: $F(t)$ – transient characteristic of the TEM horn for transmission.

The signal at the output of the receiving horn U_{out} (t) is determined by the expression (16):

$$U_{вих}(t)=h(t)E_0(t), \tag{16}$$

where: $h(t)$ – the transient characteristic of the TEM horn for reception, which in the frequency domain is determined by the formula (17):

$$h(\omega) = \sqrt{\frac{2\pi \cdot c \cdot Z_a \, r \cdot U_{out}(\omega)}{j\omega Z_0 U_{in}(\omega)}}, \qquad (17)$$

where: де $Z_a = R_a + jY_a$ – antenna impedance,

R_a – radiation resistance of the antenna,

$Z_0 = 120\pi$ – wave resistance of free space,

$j = \sqrt{-1}$ – complex unit

$\omega = 2\pi f$ – cyclic frequency.

The peculiarity of the given design is the ability to ensure the measurement of strong pulsed electric fields. Traditional antennas, on the contrary, are not capable of measuring strong electric fields, in addition, they have a complex frequency response, which complicates the process of measuring pulsed fields.

Another version of the TEM horn is presented in Figure 8.

Figure 8. TEM horn antenna [227]

The characteristics of some types of TEM horn measuring transducers are given in Table 6.

Table 6.

The characteristics of some types of TEM horn measuring transducers

Antenna, manufacturer	Conversion factor., K_n, V/(V/m)	Rise time transient characteristic, ps	Decline, ns
TEM-1, Farr Research (USA)	$1{,}8 \cdot 10^{-2}$	30	2
TEM-2, Farr Research (USA)	$3{,}5 \cdot 10^{-2}$	40	4
ИППЛ-Р, All-Russian Institute of Optical-Physical Measurements	$9{,}5 \cdot 10^{-3}$	50	2,5
Resistive Tapered TEM-horn, NIST (USA)	$1 \cdot 10^{-1}$	170	8,0

The most powerful currents are characteristic of lightning, therefore, for measuring the parameters of such currents, the electric shunt must meet special requirements. The shunt must have stable metrological characteristics when measuring the current form of 10/350 μs with an amplitude of up to 200 kA, since in this mode the worst operating conditions are ensured due to the occurrence of electrodynamic forces and withstand the heating of the resistive element as a result of the flow of component C (see table 2).

The shunt can be described by an electrical model (Figure 9). Any current-carrying conductor creates a magnetic and electric field. Therefore, in the electrical circuit, this can be taken into account by adding inductance and capacitance to the purely active resistance.

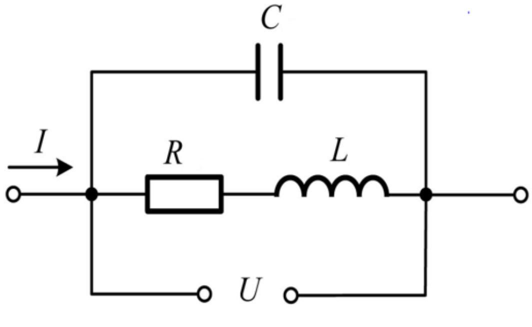

Figure 9. Electrical diagram of the shunt

For shunts with a resistance from 0.1 to 10 mΩ, the capacitive resistance 1/ωC approaches the active resistance only at frequencies above 100 MHz. [228]. In this case, the shunt voltage includes the following components:

$$u_L(t) = L di(t)/dt \; ; \quad \text{and} \quad u_R(t) = R \cdot i(t).$$

It must be taken into account that with small resistances, the inductance becomes increasingly important. The voltage on the inductance can be many times higher than the voltage on the active shunt resistance at the corresponding frequency. In [228], graphs of the shunt voltage are shown for a linear rising pulse front. For a shunt inductance of 10 nH, an active shunt resistance of 0.1 mΩ and a current in the circuit of 1 A, the voltage on the shunt is drawn in Figure 10. In this case, the voltage on the active resistance of the shunt $U_R = i \cdot R = 0.1$ mV, the voltage on the inductance $U_L = L \cdot di/dt = 1$ mV.

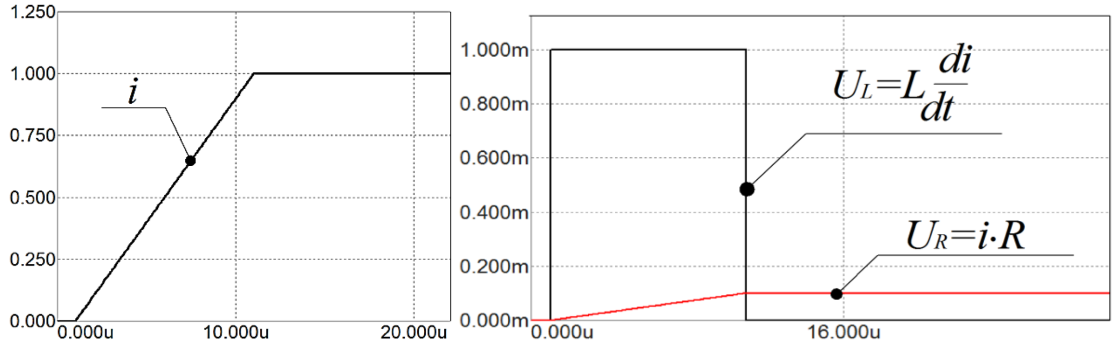

Figure 10. Graph of the voltage on the shunt for a linearly rising pulse front of 10 µs when a current of 1A flows with an active shunt resistance R = 0.1 mΩ and shunt inductance L = 10 nH [228]

In real conditions, it is impossible to obtain such a current form. Usually, current pulses are shaped like the difference of two exponents, and have a finite current rise time. The results of the voltage measurement for a shunt inductance of 10 nH, an active shunt resistance of 0.1 mΩ and a biexponential current form in the circuit with an amplitude of 1 A are presented in Figure 11. In this case, the voltage on the active shunt resistance $U_R = i \cdot R = 0.1$ mV, voltage on the inductance UL = L·di/dt = 1.43 mV.

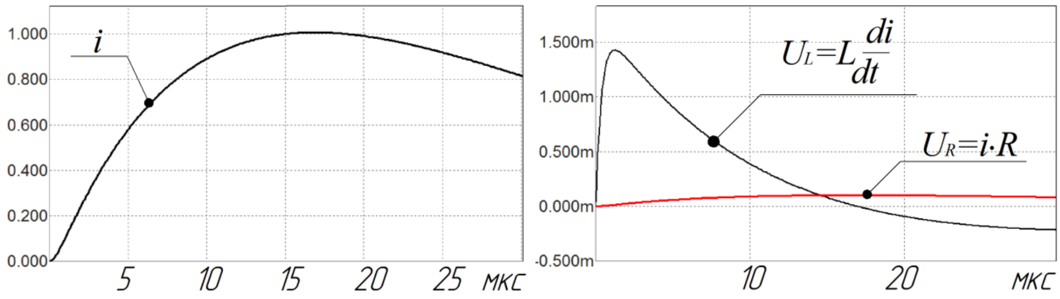

Figure 11. Graph of voltage on the shunt for a biexponential pulse with a front of 10 μs when a current of 1 A flows with an active shunt resistance R = 0.1 mΩ and a shunt inductance L = 10 nH [228]

The above shows the need to strive to reduce the inductance of the shunt. At the same time, the value of the active resistance must exceed the reactive resistance of the shunt by at least 10 times. For example, there are coaxial shunts for measuring currents up to 10 kA with active resistance from 10 mΩ to 50 mΩ with inductance from 1 nH to 3 nH.

When the current flows through the shunt, measurement errors may occur due to the skin effect and the proximity effect. These effects can lead to an increase in the active resistance of the shunt and a significant measurement error can occur. There is a sufficient number of publications and research results on these effects due to the relevance of this problem for high-frequency coils. Most analytical expressions have been obtained for inductors for various geometric parameters, but there are still no simple, theoretically justified formulas for calculating the proximity effect for arbitrary geometry. For this, computer simulation using the finite element method should be applied: COMSOL Multiphysics, ANSIS, etc.

During the flow of current in the resistive element of the shunt, as already noted, energy is released in the form of heat. When measuring currents with a large amplitude, for example, impulse currents up to 200 kA, this fact must be taken into account. The maximum heating temperature of the resistive element (ΔT) should not exceed 100 ^{0}C. For a typical value of the temperature coefficient of $5 \cdot 10^{-5}$ K^{-1}, the resistance of the resistive element increases by about 0.5%, so it does not introduce a significant error in the measurement. When measuring single pulses, the heating process is adiabatic. The power dissipated as heat in the measuring resistor can be calculated:

$$R\int_0^{t_0} i^2(t)dt = c_p m\Delta T \quad (18)$$

where: R – active resistance of the measuring resistor, Ohm;

- m is the mass of the measuring resistor, kg;
- c_p is the specific heat capacity of the measuring resistor, J $kg^{-1}K^{-1.}$

From formula (18), we can find the temperature increase ΔT (19) [229]:

$$\Delta T = \frac{J \cdot R}{m \cdot c_p} \quad (19)$$

where: J – action integral, $A \cdot s^2$;

The shape of the current pulse can be described by the equation:

$$\begin{cases} i(t) = 0,\ t < 0; \\ i(t) = k \cdot I_0(e^{-\alpha t} - e^{-\beta t}),\ t \geq 0; \end{cases} \quad (20)$$

The resistance of the disk resistor is found by formula (21) [229]:

$$R = \rho\frac{D_1 - D_2}{h\pi(D_1 + D_2)} \quad (21)$$

where: - D1 – outer diameter;

- D2 – internal diameter;
- h is the thickness of the resistive disk;
- ρ is specific resistance, Ohm m.

Based on the features of the electrical model of the shunt, taking into account parasitic effects, such as the skin effect and proximity effect and the release of energy in the form of heat, the following shunt designs are used to measure large impulse currents. The work [229] describes the design of the SHK-300M2 disk shunt for measuring impulse current up to 200 kA. Stainless steel 12X18N10T is used as a resistive element. the outer diameter of the resistive disc is 80 mm, the inner diameter is 10 mm. In [229], the calculation of the thickness of the resistive element is given under the condition that the overheating temperature should not exceed the value of 100 ^{0}C. It is shown that the thickness of the resistive disk element is 2 mm. Take into account that the process of heating the resistive element, which takes place during the duration of the electric current up to 1.0 ms, is adiabatic. The overheating temperature is limited by the type of electrical insulation. It is noted that when using fluoroplastic insulation, the overheating temperature must be chosen no more than 100 ^{0}C. The active resistance of the shunt, which was measured by the metrological service, was 0.094 mΩ.

For a resistive element with an inner diameter of d_2 = 12 mm and an outer diameter of d_3 = 100 mm, the resistance was calculated using the finite element method, taking into account the skin effect (Fig. 12). The calculation was made for nichrome material with a specific resistance of $1.1 \cdot 10^{-6}$ Ω·m for different thicknesses h_1 = 1 mm and 2 mm. For a disk with h_1 = 1 mm, the ohmic resistance is R = 0.392 mΩ, for h_1 = 2 mm R = 0.196 mΩ.

The presented data indicate that the results of shunt calibration using direct current (standard technique) have an error in determining the transformation coefficient of up to 5% (in the given case, 2.5% at a frequency of 100 kHz).

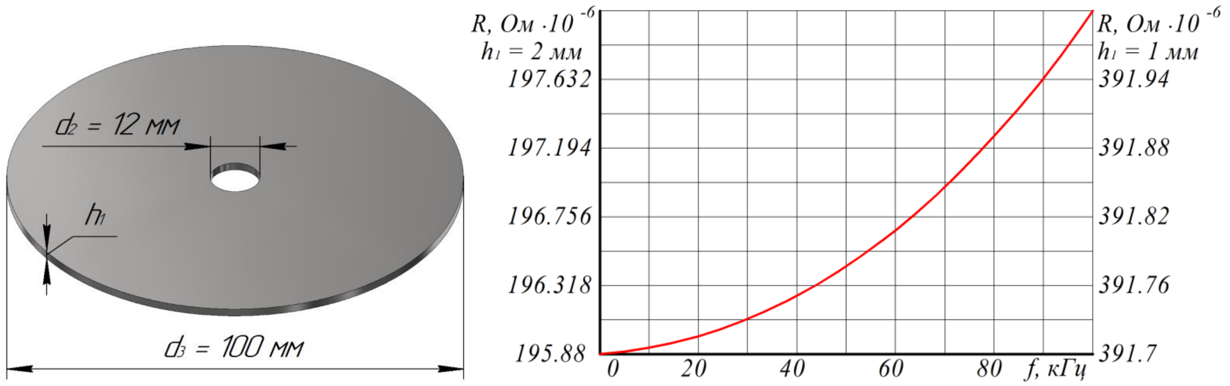

Figure 12. Dependence of the resistance of the resistive element on the frequency

Consider an alternative design [230] of a rod shunt for measuring pulsed currents of microsecond duration with a current strength of up to 75 kA. The resistive element is made in the form of segments of nichrome wire, which are located along the circumference. Calculation formulas for choosing the optimal cross-section of the resistive element and calculating the inductance are given in [230]. The sensitivity of the shunt is 350 μV/kA. Measurement of the current in the discharge circuit of the electrophysical installation showed that the front of the current pulse of 0.6 μs is transmitted without distortion.

To measure the simulated lightning current in the presence of the maximum regulated components A, B, and C, a rod-type design was chosen. The resistive resistance of the shunt was expected to be 0.1 mΩ, when the design was implemented, the ohmic resistance was 0.132 mΩ. For a rod shunt, the number of conductors is determined by the need to reduce the influence of the skin effect. This is illustrated by the following. For a conductor with radius r_0 = 5 mm and thickness l = 10 mm made of nichrome (specific resistance is $1.1 \cdot 10^{-6}$ Ω·m), the active resistance is 0.14 mΩ. The graph of the dependence of the complex resistance of this conductor on the frequency is shown in Fig. 13.

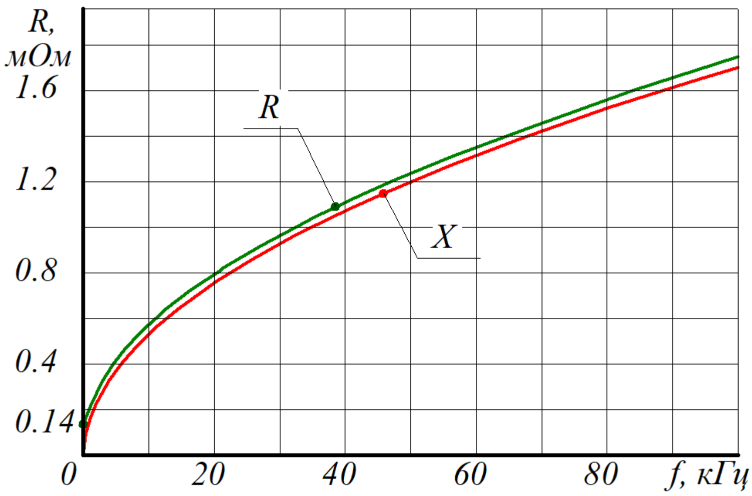

Figure 13. Graph of the dependence of the complex resistance of a conductor with a radius of 5 mm on the frequency

The graph shows that during the flow of a current pulse with a frequency of 40 kHz, which is within the time limit of the rise time of the pulse front of 10 µs, along a conductor with a radius of r_0 = 5 mm, the resistance increases almost 8 times. The design of the resistive element of the shunt is implemented using 80 nichrome conductors with a diameter of d_0 = 2 mm. In Fig. 14 shows a sketch of the resistive part of the shunt, where r_1 is the radius of the circle along which the resistive conductors are located, d_1 is the distance between the conductors. It should be noted that the distance between d_1 should be chosen so that the proximity effect does not have a significant impact.

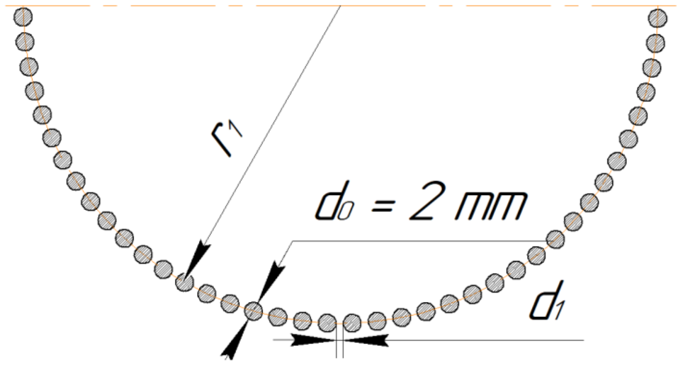

Figure 14. Design of a resistive shunt element

Figure 15 shows the graph of the dependence of the resistance of the resistive element of the shunt R on the distance between the conductors d_1 on the frequency in the range up to 100 kHz.

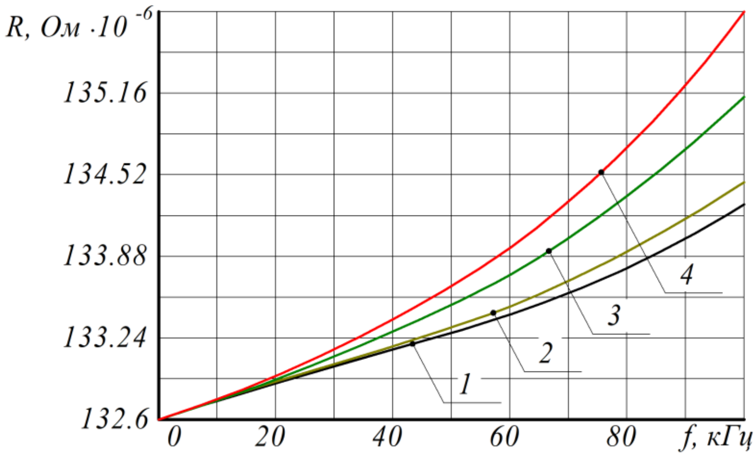

1 – d_1 = 3,5 mm; 2 – d_1 = 2 mm; 3 – d_1 = 1 mm; 4 – d_1 = 0,5 mm

Figure 15. Influence of the proximity effect for d_0 = 2 mm

It can be seen from Figure 15 that at the distance between the conductors $d_1 = 1.75 \cdot d_0$, the resistance of the conductor increases by less than 1%; at $d_1 = d_0$ by 1.8%; at $d_1 = d_0/2$ by 2.3%; at $d_1 = d_0/4$ by 3%. Depending on the specified requirements for measurement accuracy, the appropriate values of d_1 should be selected.

It is justified that for the measurement of impulse currents with a front time of 10 μs, the diameter of the conductor d_0 = 2 mm is sufficient so that the skin effect does not introduce a significant error. The distance between conductors d_1 is chosen to be $1.75 \cdot d_0$. At the same time, the proximity effect does not introduce a significant error. For the analysis of the temperature mode of operation of the shunt, the following nichrome parameters were adopted: molar mass 0.056 kg/mol; material density 8400 kg/m3; specific electrical resistance $1.1 \cdot 10^{-6}$ Ohm·m; molar isobaric heat capacity 25.2 J/(mol·K); specific heat capacity 450 J/(kg·K).

For the design of the resistive element of the shunt, which consists of 80 nichrome conductors with a radius of r_0 = 2 mm, the heating temperature of the conductor was calculated according to formula (19) and the finite element method, taking into account the skin effect and the proximity effect. At the same time, the action integral J takes a value of $10 \cdot 10^6$ $A^2 \cdot s$, which corresponds to a pulsed current with an amplitude of 200 kA and a front time of 10 μs and a decay time of 350 μs.

The heating temperature of the resistive element of the shunt, calculated according to formula (19), was ΔT = 50 °C. The value ΔT = 46.7 °C was obtained during calculations using the finite element method. The temperature distribution on the shunt structure, obtained during calculations using the finite element method, is shown in Figure 16 a). The graph of the dependence of temperature T on time is presented in Figure 16 b) during the flow of a biexponential pulse i(t) with a form of 10/350 μs.

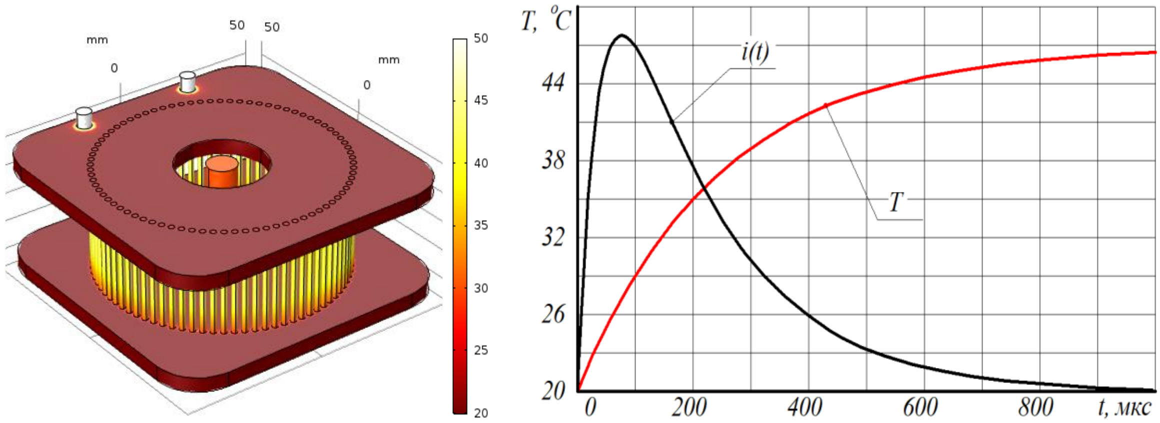

a) b)

Figure 16. Temperature field of the shunt

It can be seen that due to the selected design of the shunt, it is possible not to exceed the temperature of the resistive element of 100 ^{0}C. For a resistive disc with d_2 = 12 mm and d_3 = 100 mm made of nichrome, the heating temperature of the conductor was calculated according to formula (19) and the finite element method, taking into account the skin effect for the integral of the current action $J = 10 \cdot 10^6$ $A^2 \cdot s$. The calculation according to formula (19) does not take into account the uneven spread of the current, so it allows you to estimate only the average temperature of the resistive element. For a nichrome disk with a thickness of h_1 = 1 mm, the average temperature was ΔT = 65 ^{o}C. Figure 17 shows the temperature field of disk elements of shunts with a thickness of 2 mm (a) and 1 mm (b) for a time instant of 1 ms. The temperature distribution along the radius for different moments of time is presented in Figure 18.

The current spreads unevenly across the resistive element. This leads to uneven heating, and when the thickness of the disc $h_1 \leq 1$ mm and the resistance of the resistive element is about 0.2 mΩ, there is local overheating with a temperature higher than 150 ^{0}C. This can cause the active shunt resistance to increase significantly over time due to contact burn-in.

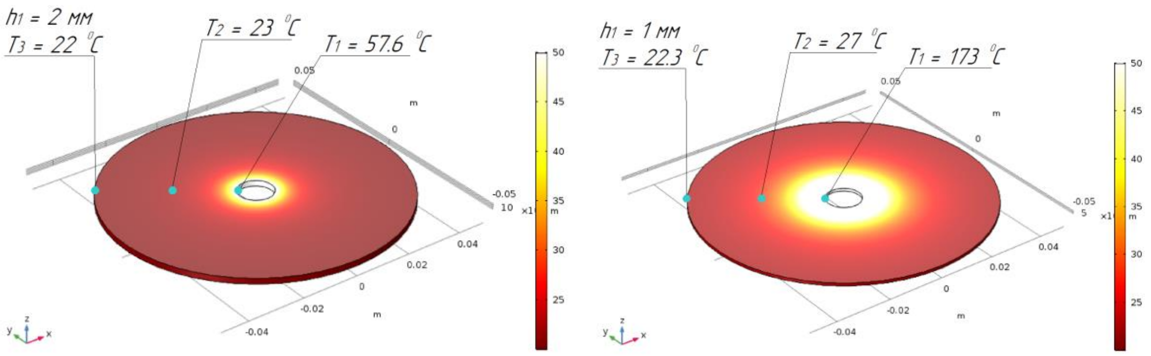

a) thickness 2 mm　　　b) thickness 1 mm

Figure 17. Temperature field of disk shunt

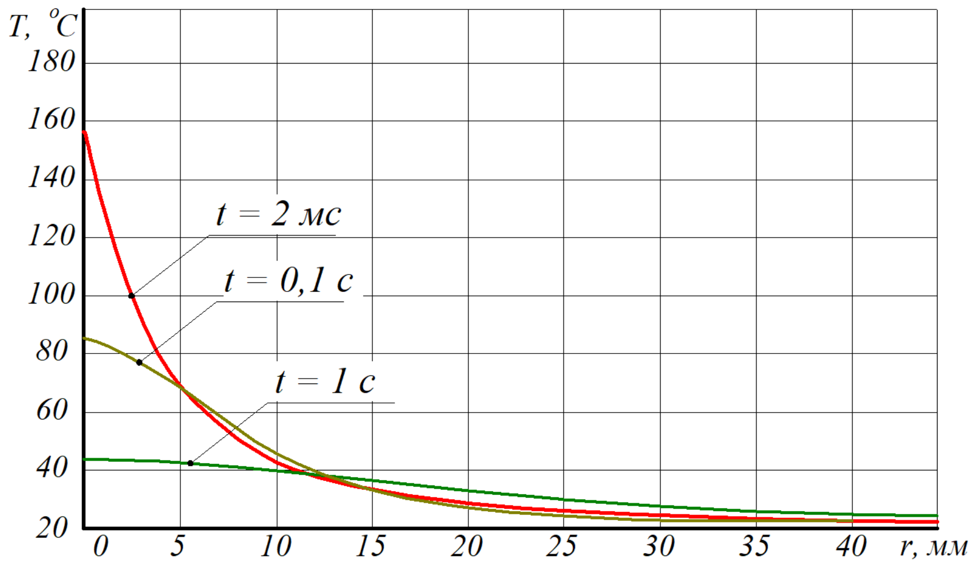

Figure 18. Temperature distribution along the radius of a disk with a thickness of 1 mm

To confirm the calculations of the heating temperature of the shunt elements described above, a physical experiment was conducted. Two samples of resistive shunt elements were used. The first sample is a resistive disc made of nichrome with a thickness of h_1 = 0.15 mm with an inner diameter of d_2 = 5 mm and an outer diameter of d_3 = 120 mm. The second sample is a wire made of nichrome with a radius of r_0 = 5 mm and a length of 140 mm. A photo of the samples fixed on the test table is presented in Figure 19.

Samples of the resistive element were connected to the discharge circuit of the pulse current generator. The temperature of the samples was measured using a Xintest HT-2 thermal imager. The parameters of the thermal imager are as follows: thermal sensitivity 0.15 ^{0}C, temperature measurement range from -20 to +300 ^{0}C, temperature measurement accuracy ±2 ^{0}C, it is possible to adjust the emission coefficient from 0.1 to 1, image capture frequency 6 Hz. The initial temperature distribution was 29.3 ^{0}C (the value is determined at the point of intersection).

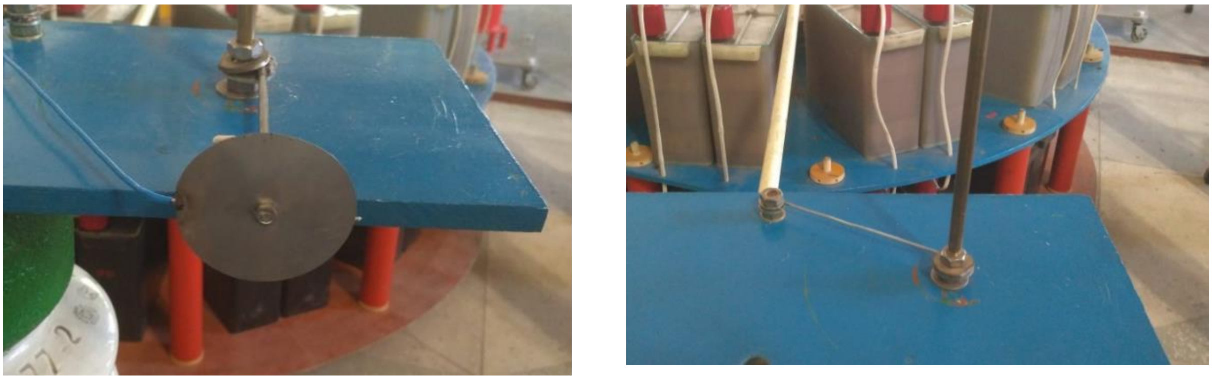

Figure 19. Photo of the samples fixed on the test table

Resistive disk. To measure the heating temperature of the resistive disk, two variants of the test were carried out, as shown in Figure 20. The variants differ in the number of current output points: 4 (a) and 1 (b).

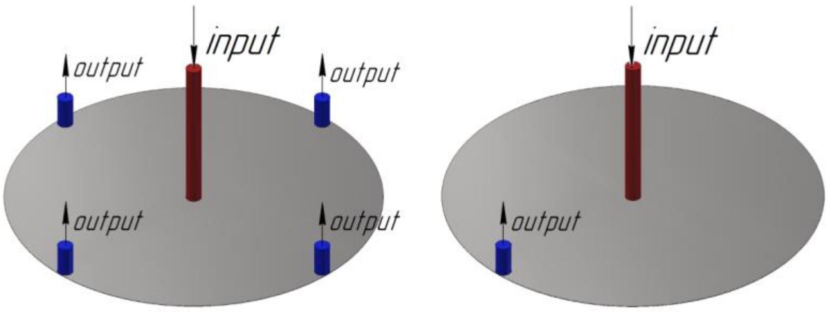

а б

Figure 20. Test options

The test results according to option a) are shown in Figure 21 for a discharge current of 28.44 kA (oscillogram on the left), the temperature determined by a thermal imager is 32.7 ^{o}C. It should be noted that the thermal imager registers the average temperature of the object, because it is at a distance of 3 m. Approaching the test area is prohibited by safety regulations and the limitation of operating conditions of the thermal imager regarding the level of magnetic field intensity.

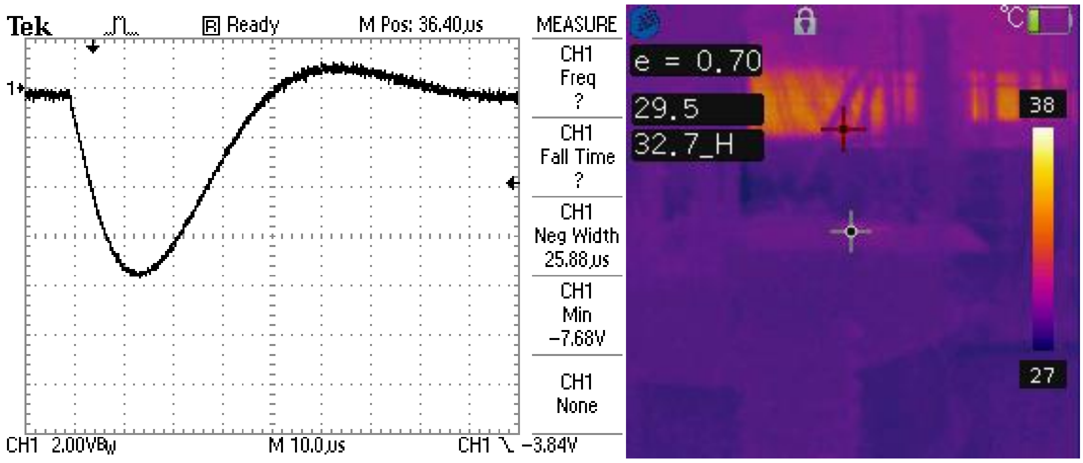

Figure 21. Oscillogram of the current of 28.44 kA and the result of measuring the temperature of the sample according to option a)

Calculation by the finite element method for the considered option is shown in Figure 22, which shows the temperature distribution along the radius of the disk for a line directed to one of the output contacts. Calculation of the temperature field of the disc element shows that the overall temperature increase is insignificant, so the thermal imager did not record local heating.

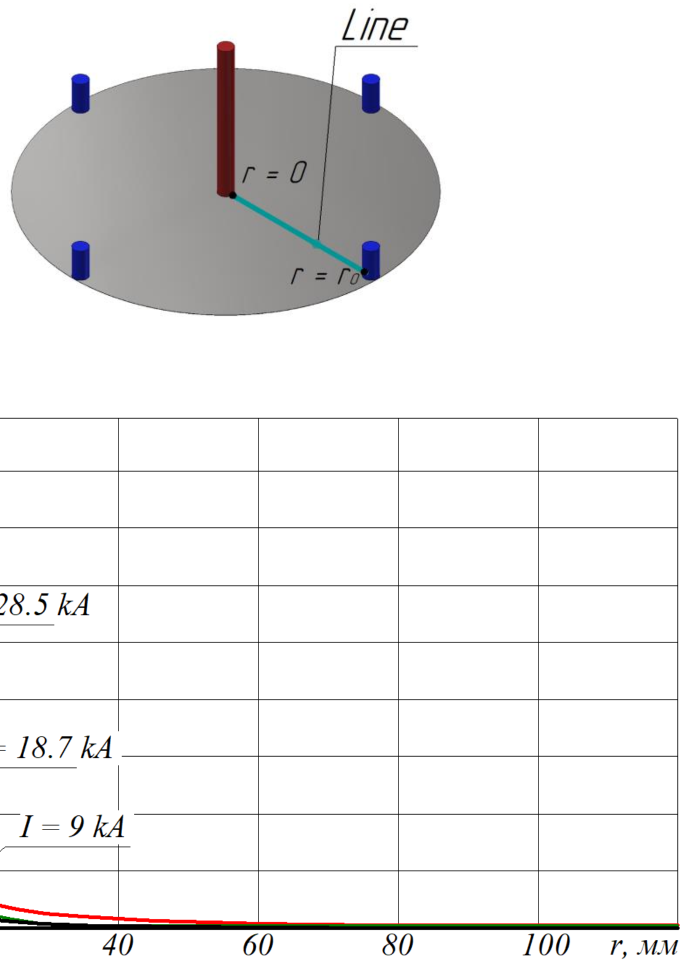

Figure 22. Temperature distribution along the disk radius

The results of the test according to option b) are shown in Figure 23, which shows the oscillograms of the discharge current and temperatures measured by a thermal imager for three values of the current strength. The calculation of the distribution of the temperature field on the sample for a time instant of 1 ms is shown in Figure 24.

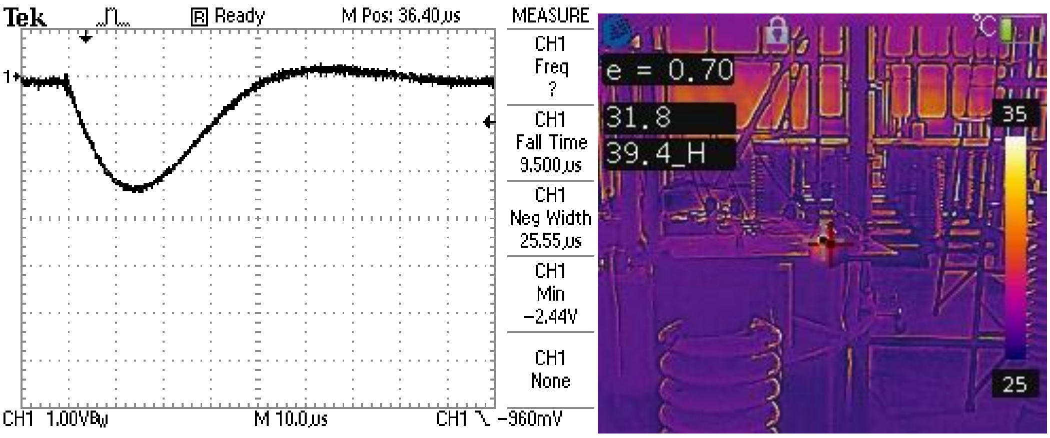

Current 9 kA

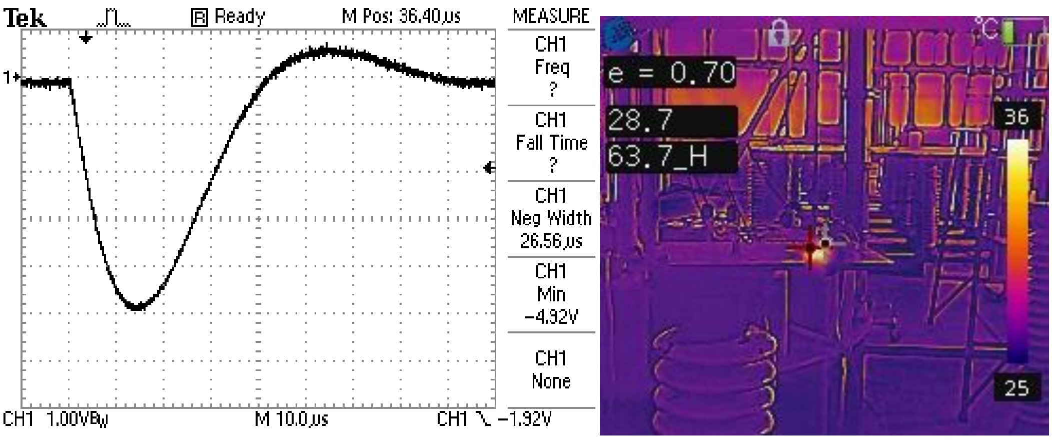

Current 18,2 kA

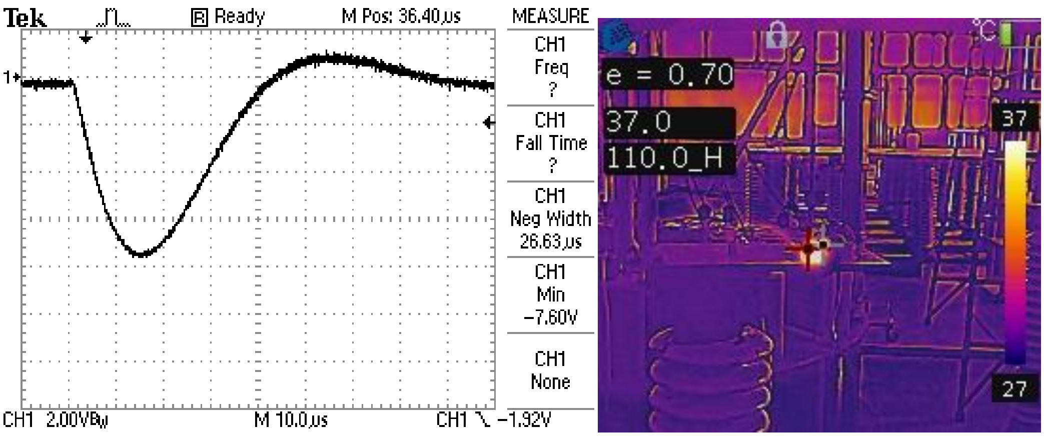

Current 28,1 kA

Figure 23. Current oscillograms and the result of measuring the temperature of the sample according to option b)

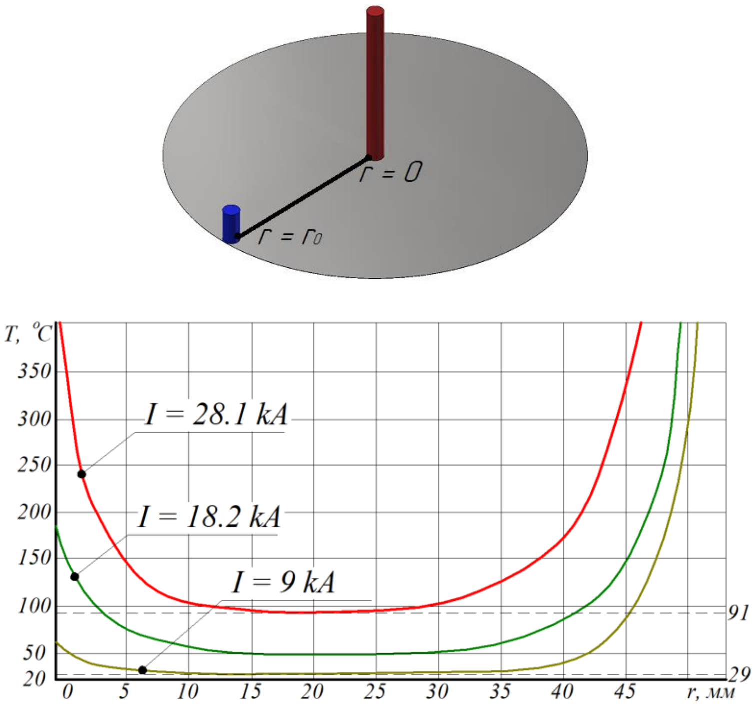

Figure 24. Temperature distribution along the disk radius

for a time, instant of 1 ms

On the thermograms from the thermal imager, it can be seen that the cursor for calculating the temperature is tied to a point that is located approximately between the input and output of the current. And it is necessary to take into account that the thermal imager recorded the temperature field at the moment of time ≈ 0.5 s. During this time, the temperature was distributed between the current inputs and the sample. The sample cools quickly due to its low heat capacity. When comparing the calculated and measured data, it can be seen that the thermal imager recorded a temperature increase of ΔT = 7.6 ^{0}C for a current of 9 kA. According to the results of the calculation for other currents, the temperature increase is for the current 18.2 kA from the thermogram ΔT = 35.0 ^{0}C, from the calculation ΔT = 28 0C; for a current of 28.1 kA from the thermogram ΔT = 73.7 ^{0}C, from the calculation ΔT = 71 ^{0}C. The difference between experimental and calculated data does not exceed 15%.

It should be noted that when the current strength increases and, accordingly, the overheating temperature increases, the difference increases due to the fact that the cooling process is carried out faster than the thermal imager records the temperature.

Flow of pulsed current along a circular conductor. For a round conductor, the overheating temperature was calculated according to formula (19). For a current form of 10/350 μs, the overheating temperature for 9 kA is ΔT = 50.2 0C; for 18 kA ΔT = 204 0C. When calculating by the finite element method, the following values were obtained: for 9 kA ΔT = 56 0C; for 18 kA ΔT = 222.4 0C. Oscillograms of discharge current and temperature measured by a thermal imager are presented in Figure 25.

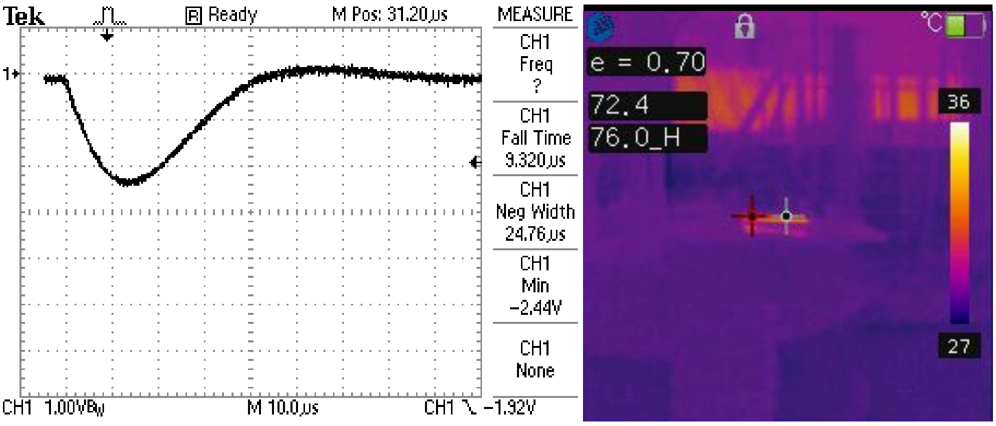

Current 9,0 kA

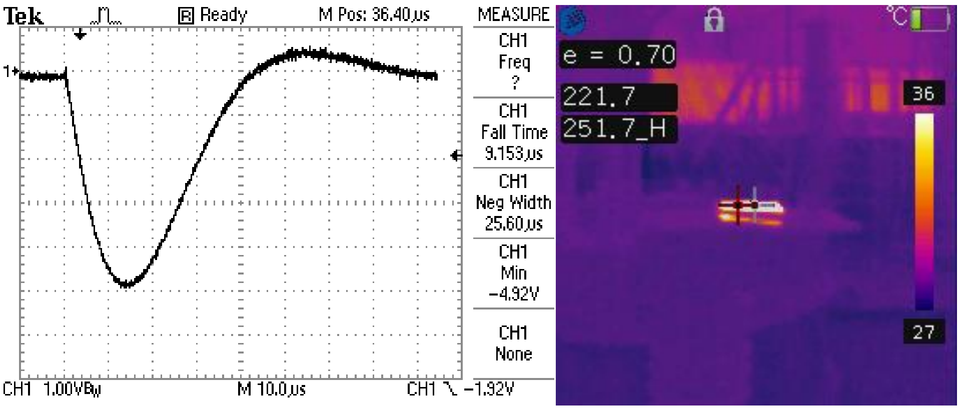

Current 18,0 kA

Figure 25. Oscillograms of the discharge current and the temperature measured by a thermal imager for a circular conductor

The results of temperature measurement showed that the overheating temperature for 9 kA ΔT = 42.9 ^{0}C; for 18 kA ΔT = = 222.2 ^{0}C. The difference between experimental and calculated data does not exceed 10%.

From the given data, it is clear that both considered shunt designs can be used to measure large impulse currents. Each design has its advantages and disadvantages.

A disc shunt has a smaller inductance and smaller geometric dimensions than a rod shunt. However, when a large-amplitude current flows, significant electrodynamic forces arise, so this fact must be taken into account during design. This fact is confirmed by the results obtained in the laboratory of NDPKI "Molniya", where the disk shunt was destroyed during exposure to a current with an amplitude of 200 kA simultaneously with the supply of the C component of the lightning current.

The rod shunt has a higher inductance, however, in this type of structure, there are no large electrodynamic forces sufficient to destroy the structure. Due to the design, the distribution of the thermal field is uniform, in contrast to the disk shunt.

Based on the results of the research, the following conclusions should be drawn:

1. It has been established that mathematical modeling is necessary to determine the parameters of disturbances that occur on long cable lines during the action of electromagnetic fields of natural and artificial origin. The need is not due to the possibility of carrying out appropriate physical modulation.

2. To take into account the real spatial arrangement of cables, which is usually complex in three-dimensional space, placed in the body of aerospace equipment, analytical formulas are not sufficient to ensure high reliability of the results. It is shown that the application of mathematical models of numerical methods is promising and requires appropriate development.

3. Experimental studies of the immunity of aerospace engineering objects to the influence of powerful electromagnetic interference regulated by current standards require the use of specialized measuring equipment. It is shown that taking temperature effects into account can lead to an error of up to 5% in the results of measuring lightning current. Which, taking into account other influences, leads to going beyond the limits of the error regulated by the standards.

4. A number of aspects related to the improvement of the technology of applying physical and mathematical models to increase the electromagnetic stability of aerospace engineering samples are highlighted.